

Recent Progress in High Power Heating and Long Pulse Experiments on EAST

Jiangang Li and Baonian Wan for the EAST team and international collaborators *
Institute of Plasma Physics, Chinese Academy of Sciences, Hefei, China

e-mail of corresponding author: bnwan@ipp.ac.cn

Abstract: New capabilities including RF powers and diagnostics have been developed since last IAEA meeting. Totally about 3MW heating and current drive power is injected into the EAST plasma. Behavior of basic plasma confinement/transport under the condition of dominant electron heating and low momentum input is investigated, which shows typical L-mode characteristics and consistent with GLF32 transport model. Divertor performance has been systematically assessed for both SN and DN configurations with normal and reversed Bt directions. Intriguing findings, particularly, in asymmetries correlated with classic drift and in control by gas puffing at various divertor locations are studied. 1MW LHW power injection has produced fully non-inductive plasma discharges, where both plasma and all PF coils can reach steady-state. Such discharges have been readily extended well over one minute. Higher power up to 1.5MW led over current driven. ICRF experiments have been conducted in different heating scenarios. Up to 2.4MW of ICRF power was injected into machine. However, weak coupling prevented effective heating. Intrinsic toroidal rotation and momentum study in ohmic and LHCD plasmas reveals the importance of the balance between the neoclassical viscosity and the neutral friction at edge. Novel wall conditioning techniques using RF and high frequency HF glow discharges in the presence of toroidal magnetic fields have been successfully applied routinely to achieve a good wall condition. Great efforts are being dedicated to high power heating, under well conditioned wall to achieve high performance plasma performance.

1. Introduction

EAST (Experimental Advanced Superconducting Tokamak) as a full superconducting tokamak has some of features similar to ITER. It was built to aim at long pulse operations over 1000s with plasma current $I_p \sim 1$ MA, and high performance plasma [1,2], thus providing a unique platform to address some of physics and engineering issues for the next step high powered long pulse fusion devices such as ITER. For example, EAST has a flexible poloidal field control system to accommodate both single null (SN) and double null (DN) divertor configurations. The divertor geometry has adopted ITER-like vertical target structures, which may demonstrate some important divertor scenarios compatible to steady-state requirements. Optimization of plasma start-up scenarios to minimize superconducting PF coil AC lose may support the ITER future safe operation.

Rotation is important for confinement, stability and access to the H-mode [3 and therein]. In an alpha-heated burning plasma the momentum input is expected to be small. The NBI power is not high enough to drive significant rotation due to the high injection energy needed for the beam to penetrate deep into the plasma. There has been a growing interest in the intrinsic rotation, namely rotating in the absence of momentum sources [4]. Intrinsic rotation associated with lower hybrid current drive (LHCD) has been observed on Alcator C-Mod [5]. Recent experiments indicate that a toroidal momentum pinch is necessary to explain the measured momentum transport. One unknown is the boundary condition for the intrinsic rotation and momentum transport. With an edge momentum source diffusion alone can then create a flat rotation profile while a pinch is needed for a peaked profile. New capabilities

developed in last two years allow us to investigate these ITER relevant issues.

2. Capability development on EAST

A significant upgrade was made since last IAEA-FEC meeting to enhance the research capability on EAST. The in-vessel components were modified to eliminate the faults found in first two campaigns with graphite as material of plasma facing components. These modification allow the machine operation in such a way that the double layer vacuum vessel is actively water cooled to maintain low thermal radiation to the thermal shield of the magnets, while the first wall can be kept hot (up to 250°C). It is essential for recycling control in long pulse discharges. The internal toroidal cryopump installed under the lower outer divertor target plate was in operation to facilitate density control and impurity exhaust.

A new ICRF heating system with total generator power of $3 \times 1.5 \text{ MW}$, frequency of 25~70 MHz is available since the beginning of 2010. Two actively cooled loop antenna with two current straps were newly installed in port I and O. The current straps of antenna on port I are fed from ends and grounded at center. This antenna is powered by two generators with variable phase shift for heating and current drive. The antenna on port O is folded, end grounded with a central current feed. Feeding and ground of two current straps are mechanically top-bottom inversed, being an out-phase configuration. Both current straps are fed by one power generator with a 3db power divider. This antenna is used only for heating. Both current straps and Faraday shielding of two antennas are made of stainless steel and were not coated. Modification of the LHCD system, mainly in detection/protection system and high voltage power supply and its control, allows higher power operation than before.

A multipurpose gas fuelling system has been installed with locations distributed at midplane of the high field side and the low field side, the upper and lower divertors from the inner divertor, the outer divertor and the central dome in the private flux region, etc. This allows the introduction of both D_2 and impurities, *e.g.*, CH_4 , N_2 , Ne and Ar *etc.*, from the different poloidal positions to study gas fuelling efficiency, impurity screening and actively control divertor asymmetry and power loading for high power long pulse operations.

An extensive set of plasma diagnostics has been installed or upgraded in EAST, which cover core and edge plasma. The core plasma diagnostics can provide most profiles of elementary parameters including the following key diagnostics: Thomson scattering system having 25 polychromators covers the half plasma vertically [6]. A new 2-dimensional soft-X crystal spectrometer with tangential view together with existing one in poloidal view provide ion temperature, toroidal and poloidal rotation velocity profiles by using Ar as tracer [7]. A new Pt foil bolometer array has 24 spatial channels covering half plasma in a poloidal cross-section. For edge divertor physics studies, following key diagnostics are newly installed: 2 sets of reciprocating probes toroidally 90° separated at the mid-plane, several filter-scope arrays monitoring D_α and CII/CIII line emissions, viewing the lower outboard divertor from the top port of the machine; the inner target and dome surfaces of both upper and lower divertors from the outer midplane through the in-vessel reflection mirrors; and 8-channel visible bremsstrahlung for Z_{eff} .

3. Experiments in last two years

3.1 Divertor experiments

EAST has a flexible poloidal field control system to accommodate both single null (SN) and double null (DN) divertor configurations [8]. The divertor geometry has adopted ITER-like vertical target structures with tightly fitted side baffles and a central dome in the private flux region to physically separate the inboard and outboard divertor chamber, and to minimize the leakage of neutrals to the main chamber. The vertical target configuration exhibits some specific attractive features [9] like: reducing peak heat load on the divertor target plates, improving divertor pumping efficiency, promoting partial detachment near the strike points, which are essential for long pulse plasma discharges.

The first experimental assessment of the divertor performance has been systematically carried out on EAST. We first studied the basic divertor plasma behaviors under Ohmic mode operating conditions, and demonstrated the plasma detachment process. Comparisons have also been made between SN and DN divertor configurations. To better understand divertor asymmetry and effect of classical drifts, we have carried out a dedicated field reversal experiment. In addition, we have investigated the effect of localized divertor puffing from various divertor locations, i.e., inner divertor, outer divertor and private flux region, using a newly developed multipurpose gas fuelling system. Furthermore, we have assessed the effect of the divertor cryopump, and carried out some preliminary studies on divertor screening for the intrinsic carbon impurity with methane puffing and the radiative divertor experiment with argon injection [10].

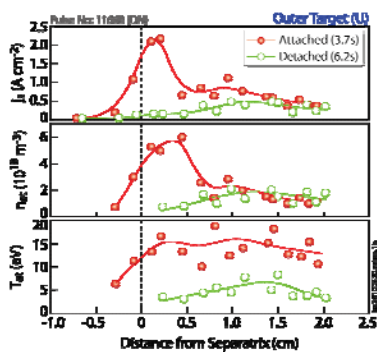


Fig. 1 Profiles of j_s , n_{et} and T_{et} along the outer divertor target plate for shot 11688 during attached and detached phases.

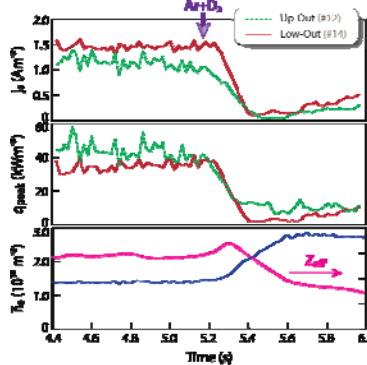


Fig.2 Effect of Ar:D₂ mixture gas injection into upper and lower outer divertors for a typical DN Ohmic discharge

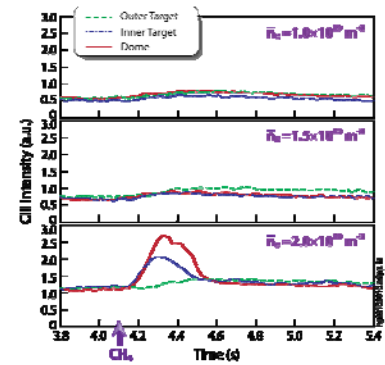


Fig.3 Changes in CIII intensity with CH₄ puffing at outer target, inner target, private flux region (dome) in DN plasmas

Partial divertor detachment near the strike points can be readily achieved in Ohmic and L-mode discharges by ramping up plasma density. DN operation exhibits an up-down divertor asymmetry with higher power and particle fluxes to the divertor target plates with their ∇B drift towards the X-point at the bottom. Detachment starts near the strike point, then expands further out along the divertor target, as plasma density rises. To illustrate this, Fig. 1 shows the profiles of ion saturation current density, j_s , electron density n_{et} and temperature, T_{et} , along the outer divertor target, at two different times, i.e., 3.7 s and 6.2 s, corresponding to attached and detached phases. As can be seen, the peak heat flux near the strike point on the target plate is greatly reduced at detachment.

However, that at large heating power, the edge density needs to be sufficiently raised to achieve divertor detachment. This may not be compatible with high confinement modes and affects LHCD efficiency. Therefore, highly radiative impurities such as Ar must be injected in divertor plasmas to promote detachment at lower densities. This experiment was conducted by injecting the $D_2+5.7\%$ Ar mixture, under steady Ohmic discharge conditions with active divertor pumping. Figure 2 shows the time evolution of an Ar seeded discharge with the Ar: D_2 mixture being simultaneously injected into the upper and lower divertor plasmas near the outer strike points for the DN configuration with the normal B_T direction. Gas puffing was initiated at 5s for duration of 0.3s at a puff rate of 8.19×10^{20} particles/s. This led to detachment at both upper and lower outer divertor targets, significantly reducing the peak heat fluxes, q_{peak} , near outer strike points. It is remarkable that despite the presence of Ar, Z_{eff} in the core plasma is actually reduced, resulting from the increase in central plasma density.

All plasma-facing components in EAST are covered with graphite tiles, so carbon is the dominant intrinsic impurity. For assessing divertor screening efficiency, a series of DN Ohmic discharges ($I_p = 250$ kA, $B_T = 2$ T) were carried out with a small amount of trace methane, CH_4 , being injected at various divertor locations. Figure 3 shows the time evolution of CIII measured at the outer midplane under different operating conditions. Divertor exhibits strong screening for carbon with little changes in CIII intensity following the injection of CH_4 , except for the higher density case, *i.e.*, $\bar{n}_e = 2.0 \times 10^{19} \text{ m}^{-3}$, CH_4 puffing at the inner target, and especially the dome.

The first comparison was made between SN and DN in Ohmic discharges. Figure 4 shows the time evolution of two density ramp-up discharges with $I_p = 250$ kA, $B_T = 2$ T (clockwise, with $\mathbf{B} \times \nabla B$ drift toward the lower X-point) for SN and DN, respectively. For a given density, particle fluxes to outer divertor targets appear to be comparable between SN and DN cases, as observed in DIII-D [11]. However, DN operation leads to a stronger in-out divertor asymmetry, which suggests a significantly lower particle loss through the inboard separatrix. In contrast, the divertor asymmetry is reduced for SN, possibly due to fast parallel transport along SOL. Strong turbulent fluctuations are present in the outer divertor for both DN and SN, most likely associated with bad curvature [12], which, at least in part, contributes to the higher particle loss through the outboard separatrix.

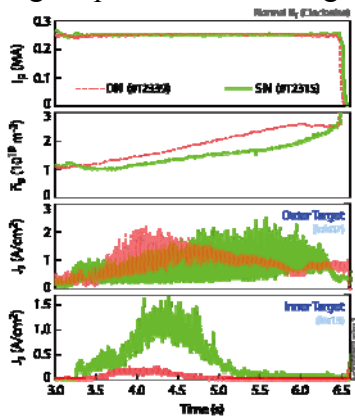


Fig.4 Time evolution of two comparable SN and DN discharges with density ramp-up.

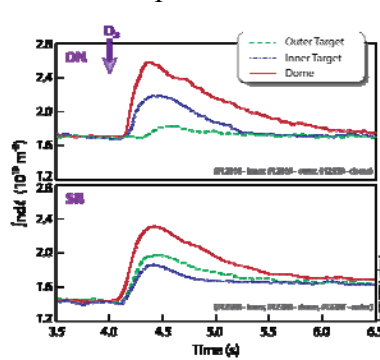


Fig. 5 Time evolution of line integrated density with localized D_2 puffing at outer, inner target and dome, for SN and DN Ohmic discharges

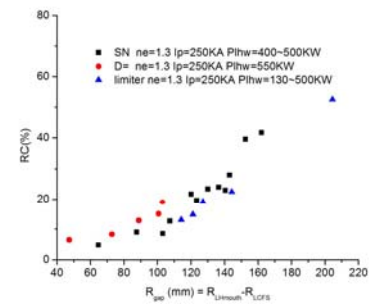


Fig.6 LHW power reflection coefficient vs distance between LCFS and the mouth of launcher in SN, DN and limiter configurations

The underlying mechanism for divertor asymmetry is still not fully understood [13]. To investigate the effect of classical drifts on divertor asymmetry, a series of dedicated experiments were conducted in EAST for both DN and SN configurations with normal and reversed B_T directions. The results shows that, for the normal B_T case, more particles go to the lower divertor target, *i.e.*, in the ion $\mathbf{B} \times \nabla B$ direction. Reversing the B_T direction appears to reverse the imbalances between top and bottom, except at very low densities. Since up and lower DN divertor magnetic topologies appear to be well balanced, this clearly demonstrates the role of classical drifts. For DN Ohmic discharges, the plasma almost disappears at inner divertor targets, therefore, it would be difficult to sustain such a poloidal $\mathbf{E} \times \mathbf{B}$ flow at the inboard divertor. In this case, the ion ∇B drift, whose polarity is in accordance with the experimental observations, appears to offer a plausible explanation. For SN, reversing the B_T direction leads to a further increase in the particle flux at the outer divertor target, most likely driven by $\mathbf{E} \times \mathbf{B}$ drifts through the private flux region. This triggers an abrupt transition to detachment at both outer and inner divertor targets, accompanied by a simultaneous increase in the core plasma radiation, ultimately reducing the density limit.

Localized D_2 puffing from various divertor locations has also been carried out to investigate divertor closure for neutrals and gas fuelling efficiency under typical Ohmic discharge conditions. Figure 5 shows the time evolution of line integrated electron density, with D_2 puffing at outer and inner divertor targets, as well as dome, for both DN and SN divertor configurations. As can be seen, D_2 puffing from the dome leads to a large increase in line integrated electron density in both cases, suggesting strong leakage of neutrals from the private flux region. For the DN configuration, there appears to be a strong asymmetry in gas fuelling efficiency between inner and outer divertor gas puffing, with a significantly higher density rise following inner divertor puffing, thus indicating poor divertor closure for neutrals from the inner divertor target. However, for SN, the gas fuelling efficiency appears to be similar between inner and outer divertor target gas puffing.

3.2 LHCD experiments and long pulse plasma discharges

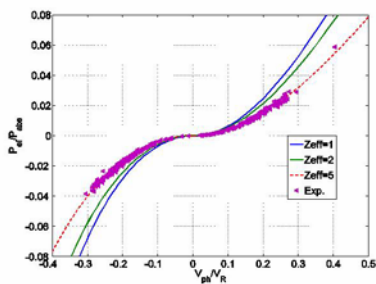


Fig.7 Experimental data of P_{el}/P_{abs} versus V_{ph}/V_R which are fitted to theory curves with Z_{eff} dependence.

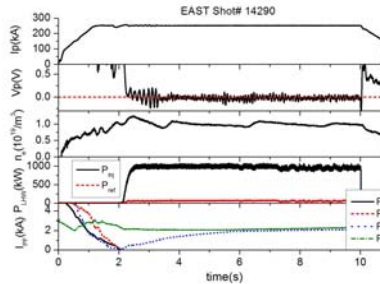


Fig.8 A fully non-inductive discharges by LHCD. All PF current after 6s are kept unchanged.

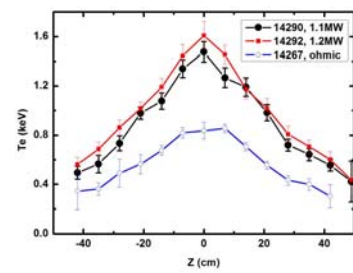


Fig.9 electron temperature profile for shot shown in Fig.8 and compared with an ohmic shot and an over current driven shot.

The LHCD experiments have firstly performed using the iso-flux shape control algorithm to optimize the coupling of LHW power into plasma. It was also done through regulation of the gap between LCFS and the mouth of launcher in different configurations. The best coupling is obtained in the limiter case as seen in Fig.6. This observation could be well explained by the

magnetic connection length [14]. A good coupling with $RC < 10\%$ at gap distance less than 10 cm has been obtained for most LHCD experiments.

The current driving efficiency under different configuration has been accessed by LHW power scanning. It is found that LHCD efficiencies in SN and DN configurations are comparable, but higher than one in limiter configuration for the plasmas having same current and the line averaged density. It is observed that the internal inductance is decreased from ~ 1.8 of ohmic plasma to ~ 1.55 of fully non-inductive discharge at $I_p=250\text{kA}$ and $\bar{n}_e=1.0*10^{19}\text{m}^{-3}$, in DN configuration. This implies off-axis current carried by LHW driven fast electrons, which the code simulation using LUKE/C3PO code shows a peak of power deposition at $\rho \sim 0.4$ for such plasmas [15]. LH wave power deposition in confinement region causes significant electron heating, while ion heating is very weak. It is mainly due to the fact that an increased energy transfer to ions by collisions is almost compensated for by less frequent collisions and decreased energy confinement time at higher LHW powers[16]. The confinement/transport analysis shows that such plasmas with LHW has typical L-mode characteristics and consistent with GLF32 transport model [17,18].

Based on the theory of conversion of LH wave energy into poloidal magnetic field energy, the experimental results at $I_p=250\text{kA}$ and $\bar{n}_e = 1.0*10^{19}\text{m}^{-3}$ in DN configuration are plotted in [fig. 7](#), where P_{abs} , P_{el} , V_{ph} , V_{R} are defined in [19]. From fitting of data, fraction of absorbed power of ~ 0.8 and factor of power spectrum up-shift of ~ 1.5 can be deduced. The discrepancy of current driven efficiency in different configuration can be roughly explained by up-shift factor of wave power spectrum [20]. Note that data shown in [fig.7](#) include these shots with over-current drive, where $V_{\text{ph}}/V_{\text{R}}$ are positive. At 1MW of LHW source power, plasma current can be sustained fully non-inductive. As seen in [fig.8](#) for such a shot with the LHW applied at 2s, the surface voltage was dropped and reached to zero at about 3s and the currents in all PF coils reached steady-state at about 6s. Corresponding electron profile is shown in [fig. 9](#). Note that such a discharge is really in a steady-state status after 6s, where all key plasma parameters including β_p , l_i and plasma shape were sustained at constants. The time needed for the surface voltage dropping to steady-state is comparable to the current diffusion time. However, what is the time scale for all PF currents to steady-state, is still not clear. At even higher LHW power, the surface voltage can be dropped to negative, where an opposite ohmic current was produced, but compensated by an over current drive by LHW to maintain total constant plasma current.

Based on these experiments above, long pulse plasma discharges up to 30s were readily achieved both in SN and DN configurations, which demonstrate the capabilities of various systems, e.g. plasma control, LHCD, in-vessel components, etc. To get even longer plasma discharges, the operation scenarios were optimized. The gas puffing from the dome was used for line averaged density control because of its higher fuelling efficiency (see divertor experiments). It reduced the fuelling gas amount for same line averaged density, e.g. retention of gas, which is beneficial for long pulse discharges. DN configuration was adopted for long pulse plasma discharges because of lower peak heat load on divertor plates. Internal divertor cryopump was applied to facilitate density control and impurity exhaust. The repeatable minute scale long pulse plasma discharges were obtained at $I_p=250\text{kA}$ and $\bar{n}_e=1.0*10^{19}\text{m}^{-3}$ at the condition of the PFC without active cooling. As seen in [fig. 10](#), the plasma current and line averaged density were quite well feed-back controlled. The slow temporal variation in R and Z of the last closed magnetic flux surface were pre-set for swinging the strike points along the divertor plates. It was do so to avoid the heat peak at the same location during whole discharge duration. Despite strike point swinging, the main limitation for even longer pulse is presently still heat load constraints on the divertor plates. The plasma facing components were not actively cooled in these experiments because of several small leakages

on the heat sinks and cooling tubes.

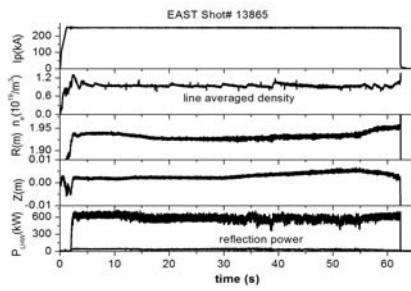


Fig.10 A minute scale long pulse discharge on EAST. Note slow variation in R and Z .

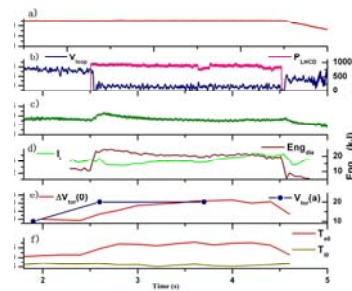


Fig.11. Evolution of the toroidal flow at center and edge of LHCD plasma.

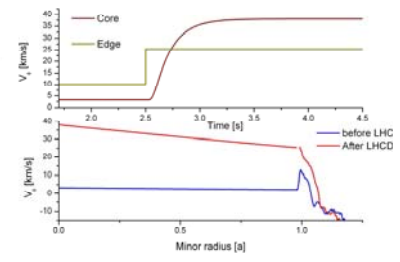


Fig.12 The simulation results based on turbulent equipartition theory and thermoelectric pinch using the experiment data.

3.3 Toroidal Rotation in LHCD plasma

Intrinsic rotation associated with lower hybrid current drive (LHCD) has been observed on Alcator C-Mod [5]. It is also observed on EAST. The toroidal flows in LHCD plasmas on EAST are non-localized and mainly in the co-current direction. In contrast, the self-generated flows in C-Mod's LHCD plasma are core localized and in the counter-current direction. Figure.11 shows the temporal waveforms of an EAST discharge in which the injection of LHW causes strong co-current flows both in core and edge region. 800kW of LHW power are coupled to 250kA plasma from 2.5s to 4.5s. The toroidal rotation were measures by reciprocating probes at $t=1.9s$, 2.6s, and 3.7s. It is seen that the toroidal rotation at edge plasma had a prompt increment in the co-current direction after the injection of LHCD, and was kept at a constant during the LHCD phase. The edge density and temperature had the same temporal behavior. On the other hand, the central toroidal rotation evolves on a considerably longer time scale than those of edge rotation, electron and ion temperature, and current redistribution time.

The loop voltage is around zero during the injection of LHCD. So the Ware pinch effect can be ignored. The fast change of edge rotation may be contributed by the parallel return 'Pfirsch-Schluter' (P-S) flows, which arise to compensate the non-divergence free poloidal $E_r \times B$ and $\nabla P \times B$ classical drift flows in toroidal geometry [21]. In the present LHCD case, the behavior of edge rotation is same as edge temperature and density. Furthermore, the decay length in SOL provided by Langmuir probe array along the divertor plates is significantly reduce during LHCD, which is consistent with P-S flows property. It seems that there is a strong correlation between the edge and core rotation, which is also observed in other LHCD shots. In the limiter LHCD shots, the core plasma rotations increased little, while the edge parameters and toroidal rotation had been changed very little.

A simple model based on turbulent equipartition (TEP) theory and thermoelectric pinch [22] may links these observations from the core and edge regions. Figure 12 shows the simulation results. In fig.12, the data of edge rotation are taken from the experimental measurements. It is seen that the core toroidal rotation evolves for about 1 s to reach steady-state, which is similar to the experimental observation. Moreover, as seen in fig. 12b, the simulated core toroidal rotation is near 40km/s and flat, which is also consistent with the experimental

results.

3.4 ICRF experiments

ICRF experiments were conducted for the first time on EAST in 2nd harmonic, minority and mode conversion scenarios. Maximum injection power of 1.6MW was achieved using antenna at port I and 0.8MW using antenna at port O. Experiments of ICRF heating at frequency of 27MHz and toroidal magnetic field of 2 Tesla are being carried on minority and mode conversion scenarios by control of hydrogen fraction in deuterium plasma using SiD4 coatings. But no clear heating either in electron or ion has been observed despite of measurable increment of plasma energy. The heating scenarios of second harmonic at 56MHz, 1.9Tesla and He3 minority at 2.6 Tesla were also tried. Again there was no obvious heating. Analysis of radiation found significant increment of metal impurity line emission. Although there is no direct measurement of coupling resistance on EAST, analysis found that the coupling of ICRF wave to plasma is rather weak, only about 0.2Ω , which is due to a large distance between the current straps and cut-off layer of the wave. This may account for “missing power” of the ICRF waves on EAST, which most power was dissipated in SOL and caused strong radiation during application of wave power. To confirm this conjecture, experiments of ICRF heating in HT-7 were analyzed and compared with that on EAST.

In HT-7 with the limiter configuration, antenna is located at the radial position only 1cm behind the limiter. The analysis deduced the coupling resistance typically at 0.4Ω , much higher than that on EAST. The antenna on HT-7 is also made of stainless steel and no coating on it. However, direct electron and ion heating has been observed in mode conversion regime, even the ratio of H/(H+D) was high at 30% [23]. Here ICW due to the effect of poloidal field in MC may be responsible for direct wave damping on ion [24].

Recently, antennas have been modified based on this analysis. Four RF probes were installed toroidally separated at the mid-plane of the vessel to confirm the RF wave power in SOL. Further effort is being dedicated to improving the coupling and different heating scenarios to address several key physical issues, such as transport control, flow driven, direct verification of poloidal field effect in MC, production of energetic particles, etc.

3.5 Effort to approach MA operation

Plasma start-up has been optimized to minimize superconducting PF coil AC lose for simulating ITER future safe operation. Low loop voltage breakdown at 0.15V/m and plasma ramping rate between 0.1MA/s and 0.5MA/s has been obtained with different shaping and assistance of LHW[25]. Utilizing features of LHCD assistant start-up, plasma current could be readily ramped up to and sustained stably at 0.8MA with a ramping rate of 0.2MA/s by shape pre-program control and feed back control of plasma current and position. Maximum current up to 0.9MA was achieved in such an operation scenario. However, such a near 1MA plasma can only be realized with a limited elongation of 1.3 in limiter configuration. Two factors are limited for even larger elongation and achievement of diverted configuration: capability of the internal coils power supply, e.g. insufficient total current and temporal response (voltage applied at the internal coils) for vertical stabilization; insufficient voltages of the PF coil power supplies, particularly, those for divertor coils and vertical field coils, for shaping.

Under this operation mode, we tried high power heating by LHW and ohmic powers. LHW was applied to assist current ramping up and heat plasma. The loop voltage was suddenly increased via the program control of PF voltages when plasma current was ramped up to 0.6MA. This increment of the loop voltage provides about 1MW heating power. Together with LHW, total absorbed power by plasma reached about 1.7MW. Both energy and particle confinement has been observed in this stage, as seen in [fig. 13](#). Presently, it is not clear whether such a confinement improved plasma has edge and/or internal transport barrier due to the limited diagnostic capabilities during this experiments.

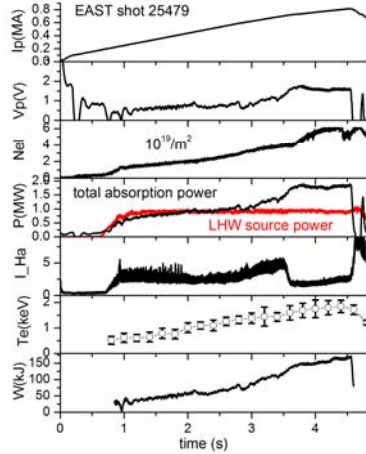


Fig.13 A high power heating plasma during I_p ramping up phase achieved improved confinement

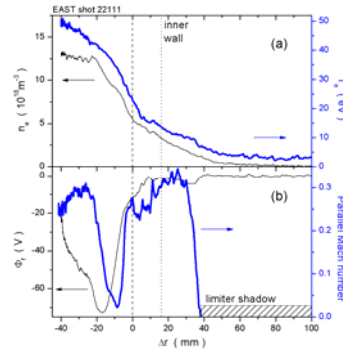


Fig.14. (a) n_e and T_e profiles, (b) floating potential V_f and parallel Mach number $M_{||}$ profiles.

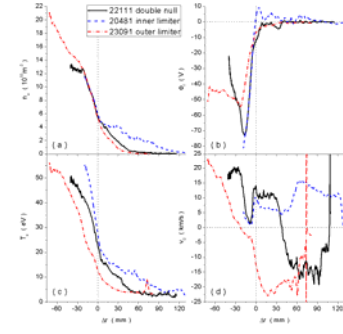


Fig.15. The radial profiles of (a) electron density (b) floating potential (c) electron temperature (d) parallel velocity.

3.5 Edge experiments

A series edge experiments were dedicated to plasma flow using two newly installed reciprocating probe systems. The bulk ion toroidal velocity (V_ϕ) in the outermost 4 cm of the confined region and in the scrap-off layer of Ohmic plasmas is measured using Mach probes. In this experiment the collisionality $\nu_i \equiv q_{95} R_0 v_{ii} / v_{thi}$ at the plasma edge is larger than 4, the edge plasma is in the Pfirsch-Schlüter regime. At about 1 cm inside the separatrix a local minimum in the V_ϕ is observed, as shown in [Fig.14](#). The radial width of the V_ϕ dip is 1~2 cm. It is situated at the same location of a dip structure in the radial electric field (E_r), where density and electron temperature profiles show steep gradients. It is observed in discharges with both divertor and inner limiter configurations but not in the discharges that the plasma edge touches the outer limiter, as indicated in [Fig.15](#). Similar dip structure in toroidal rotation was recently observed in the H-mode plasma edge of the ASDEX-U and DIII-D tokamaks [26]. The velocity increment in our experiments amounts to ~ 20 km/s, which is at the same level of those reported from ASDEX-U and DIII-D H-mode, suggesting that this is not an exclusive character of the H-mode.

The parallel Mach number in the near SOL decreases with the increase of the line-averaged density and scales linearly with the Pfirsch-Schlüter ion flow at the outboard midplane, as shown in [Fig.16](#). The neoclassical offset of the parallel velocity is more than two times larger than the measured value but the Pfirsch-Schlüter flow profiles roughly coincide with the measured flow profiles, as indicated in [Fig.17](#).

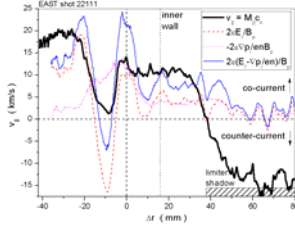


Fig.16. The parallel velocity profile and the Pfirsch-Schlüter flow profile, here the E_r is calculated as the radial gradient of the plasma potential.

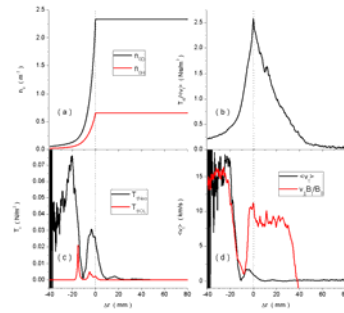


Fig.17. The radial profiles of (a) neutral density (b) toroidal velocity induced by charge exchange neutral friction and (c) by the neoclassical viscosity and the ion orbit loss (d) the toroidal velocity associated with the balance between (b) and (c)

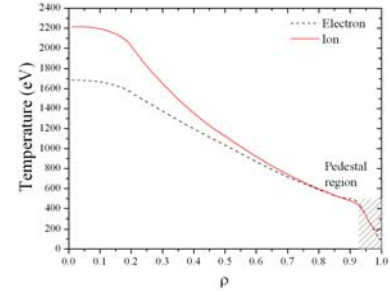


Fig. 18 Temperature profiles of the plasma with the highest stored energy.

The toroidal torques induced by the neutral friction, neoclassical viscosity, ion orbit loss and turbulence Reynolds stress are evaluated using the measured parameters. The results indicate that the neutral friction is the dominant damping force. The data indicates that at these parameters the contribution from the turbulence Reynolds stress is relatively small. The toroidal velocity assessed under the assumption that the neoclassical viscosity balances the neutral friction, $\langle v_t \rangle = T_{tNeo} / (T_{t0} / \langle v_t \rangle)$, fits the measured velocity $v_{||} B_t / B_0$ very well, as shown in Fig.17(d), suggesting that the structure in the toroidal rotation could be interpretable by the balance between the neoclassical viscosity and the neutral friction. These results are potentially important for the understanding of the boundary condition for the intrinsic toroidal momentum, or perhaps on the momentum source, in the tokamak plasmas.

3.6 High frequency glow discharges for wall conditioning

Recently, High Frequency Glow Discharge Cleaning (HF_GDC) in the presence of a magnetic field is demonstrated in the both of EAST and HT-7 Superconducting Tokamaks. Preliminary results are encouraged not only for wall conditioning, but also for pre-ionization of plasma discharges. The uniform high-frequency glow was observed around toroidal direction in the central region. HF-GDC could be applied with or without toroidal magnetic files and in a more wide rang of pressure about from several Pascal to 10^{-4} Pa both for helium and deuterium. Preliminary experiments show that the cleaning efficiency of HF_GDC is higher than that of RF_GDC with B-field. Various coating using this technique was also demonstrated to be very effective for impurity suppression.

4 Summary and near future plan

Since last IAEA meeting, significant progress in development of research capabilities, high power heating/current drive, long pulse discharge and some dedicated experiments has been

made on EAST. The basic divertor features including heat load issues, classic drift, impurity screen effect, etc have been systematically accessed. Optimization of the coupling of LHW to plasma and LHCD efficiency led to repeatable minute scale long pulse plasma discharges, coupled with some of divertor features. Presently, coupling problem of ICRF wave is still big issue to achieve effective heating for high performance plasma, although more than 3MW total heating power was simultaneously injected into the machine. EAST could be operated at near 1MA in the elongated limiter configuration with the LHCD assistance. By using combination of ohmic and LHCD power, improvement of plasma confinement has been observed at a total absorbed power of 1.7MW. New diagnostic capabilities allow us for the first time to investigate the intrinsic toroidal rotation for both core and edge plasmas.

Presently, a 2MW lower hybrid current drive system at 2.45GHz and a new 4.5MW ICRF system at 25-70MHz are available. This power should be sufficient to access the high performance regime, such as H-mode, which is predicted by pTRANS[18]. Figure 18 shows an example of a ^3He minority ($n_{\text{min}}/n_e \sim 4\%$) scenarios with line-averaged density $3.0 \times 10^{19} \text{ m}^{-3}$, effective total heating power $P_{\text{heat}}=1.9 \text{ MW}$, including $P_{\text{LHW}}=300 \text{ kW}$, $P_{\text{ICRF}}=1.4 \text{ MW}$. Some major modifications need to be made to achieve this goal. These include the ICRF antennas, PF and IC power supplies, which will be done soon. The ICRF antenna will be improved to minimize the parasitic power dissipation in SOL by aligning the cline angle of Faraday shield possibly matching to magnetic field line and to reduce the impurity sputtering by coating BC4 on the antenna surface. The voltage of divertor and vertical coil PF power supplies will be increased by 50% to enhance the plasma control ability at higher plasma current. New modules of IC power supply with higher voltage and current are under testing. In the next two years, diagnostics on EAST will also been significantly extended for some specific physical studies. The total source power for heating and current drive will be increased to 10MW.

Acknowledgements

This work was supported by the National Natural Science Foundation of China under Grant No. 10725523 and No. 10721505.

Reference

1. Y.X. Wan *et al.*, Nucl. Fusion **40** (2000) 1057,
2. BaonianWan, et al., Nucl. Fusion **49** (2009) 104011
3. P.W. Terry, Rev. Mod. Phys. **72** (2000) 109
4. J. E. Rice et al., Nucl. Fusion **47** (2007) 1618
5. A. Ince-Cushman et al., Phys. Rev. Lett. **102** (2009) 035002
6. Q.Zang et al, Plasma Sci. Tech.,**12** (2010), 144-148
7. Y.J. Shi, etc., Plasma Phys. Control. Fusion **52** (2010) 085014
8. S. Zhu and X. Zha, J. Nucl. Mater. **313-316** (2003) 1020
9. A. Loarte, Plasma Phys. Control. Fusion **43** (2001) R183.
10. H.Y Guo, et al., EXD/P3-14, this conference
11. Petrie, T.W., et al., J. Nucl. Mater. **290-293** (2001) 935. Petrie, T.W., et al., J. Nucl. Mater. **313-316** (2003) 834
12. H.Y. Guo *et al.*, Nucl. Fusion **40** (2000) 379
13. C.S. Pitcher and P.C. Stangeby, Plasma Phys. Control. Fusion **39** (1997) 779
14. Brambilla M. Nucl. Fusion **16** (1976) 47
15. Brizard A. J., et al., Phys. Plasma **16** (2009) 102304

16. X.L.Li et al., PPCF **52** (2010) 105006
17. X. Gao, et al., EXC/P4-06 this conference
18. S.Y.Ding, EXC/P2-01, this conference
19. C.F. Karney, N.J. Fisch, F.C. Jobes, Phys. Rev. A **32** (1985) 2554.
20. B.Ding et al., EXW/P7-03, this conference
21. A.V. Chankin, J. Nucl. Mater. **241–243** (1997) 299, R.A. Pitts et al., J. Nucl. Mater. **363–365** (2007) 505
22. T. S. Hahm, et al., Phys. Plasmas **14** (2007) 072302, O. D. Gurcan, et al., Phys. Rev. Lett. **100** (2008) 135001.
23. X.L.Li et al., EXW/P7-13, this conference
24. Jaeger E.F. et al Phy. Rev. Lett. **90** (2003)195001
25. B.J.Xiao, et al., EXS/P2-18, this conference
26. T. Pütterich, et al., Phys. Rev. Lett. **102** (2009) 025001. J. S. deGrassie, et al., Nucl. Fusion **49** (2009) 085020.

EAST teams and International collaborators:

- 1) Institute of Plasma Physics, Chinese Academy of Sciences, Hefei, China
- 2) Donghua University, Shanghai, China
- 3) South West Institute of Physics, Chengdu China
- 4) Tsinghua University, Beijing, China
- 5) Beijing University, Beijing, China
- 6) University of Science and Technology of China, Hefei, China
- 7) General Atomic, San Diego, USA
- 8) Fusion Research Center, UT at Austin, USA
- 9) Princeton Plasma Physics Laboratory, USA
- 10) Tri Alpha Energy, Rancho Santa Margarita, CA 92688, USA
- 11) Plasma Science and Fusion Center, MIT, Cambridge, Massachusetts 02139-4307, USA
- 12) National Institute for Fusion Sciences, Toki, Japan
- 13) Association Euratom-CEA, CEA Cadarache, France
- 14) National Fusion Research Institute, Korea Basic Science Institute, Daejeon, Korea